THE JOURNAL OF PHYSICAL CHEMISTRY B

ARTICLE

pubs.acs.org/JPCB

Counter Anion Effect on the Self-Aggregation of Dimethyl-di-*N*-octylammonium Cation: A Dual Behavior between Hydrotropes and Surfactants

Marion Collinet-Fressancourt,[†,‡] Loïc Leclercq,[†,‡] Pierre Bauduin,[§] Jean-Marie Aubry,[†,‡] and Véronique Nardello-Rataj*[,†,‡]

[†]Université Lille Nord de France, F-59000 Lille, France

[‡]Université Lille 1 and ENSCL, EA 4478 Chimie Moléculaire et Formulation, F-59655 Villeneuve d'Ascq Cedex, France

[§]Institut de Chimie Séparative de Marcoule, UMR 5257, CEA/CNRS/UM2/ENSCM, BP 17171 CEA Marcoule, F-30207 Bagnols-sur-Cèze, France

Supporting Information

ABSTRACT: Self-aggregation of eight dimethyl-di-*N*-octylammonium salts ($[DiC_8]$) has been investigated as a function of the nature of the counteranion. Tensiometry, conductimetry, and $[DiC_8]$-selective electrode measurements highlighted three different behaviors and led to a rationalization of the aggregation process depending on the counteranion: "hydrophilic" anions (MoO_4^{2-}, WO_4^{2-}, SO_4^{2-}, F^-) give only unimers and micelles, whereas less hydrated anions form unimers, dimers, and either one micelle-like structure (NO_3^-, Br^-) or two micelle-like structures ($CH_3SO_3^-$, Cl^-). Small-angle neutron and dynamic light scattering confirms the unusual behavior of $[DiC_8][Cl]$, which forms two types of aggregates: (i) disk or vesicles between 10 and 30 mM and (ii) ellipsoidal micelles above 30 mM. For $[DiC_8][MoO_4^{2-}]$, the formation of ellipsoidal micelles is supported between 10 and 300 mM. Finally, shapes and sizes of the aggregates are confirmed by molecular dynamic experiments.

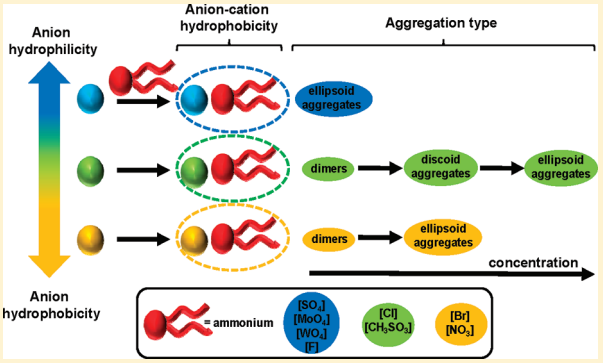

INTRODUCTION

The development of self-assembly molecules is an important field of supramolecular chemistry. Molecular recognition-directed self-organization can lead to the formation of new structures with fascinating properties.[1−4] In contrast to traditional covalent systems, the supramolecular aggregates and their properties can be externally controlled (temperature, concentration, solvent, pH, etc.).[5−8] For example, amphiphiles, which are based on hydrophilic and hydrophobic moieties, are archetypes of self-assembling molecules because their orientation and packing can be controlled by changing the concentration or the temperature.

Depending on the hydrophobic tail length, two families of amphiphiles can be distinguished: (i) surfactants and (ii) hydrotropes.[8,9] These two families present some similar properties, such as surface tension reduction or aqueous solubilization of hydrophobic molecules,[4] but the solubilization mechanisms are very different. The solubilization with surfactants is due to the formation of well-defined aggregates (e.g., micelles), whereas with hydrotropes, a specific solvation is responsible for the formation of small aggregates between solubilizate and hydrotrope molecules.[8,9] For surfactants, a critical aggregate concentration (CAC) is observed at low concentration ($\approx 10^{-2}-10^{-4}$ M), above which self-aggregation "suddenly" occurs, whereas hydrotropes present a "stepwise" self-aggregation around a solubilizate.[10−13] This "stepwise" aggregation starts at a high and ill-defined concentration (≈0.1−1 M).[14] The hydrophobic part of hydrotropes is generally too small to cause large and collective self-aggregation (e.g., micelles).

We have recently reported the peculiar conduct of dimethyl-di-*N*-octylammonium chloride ($[DiC_8][Cl]$), which presents dual behavior starting from a stepwise association, like hydrotropes, followed by a collective association, like surfactants.[15] To gain further insight into the self-association process, we have investigated the anion effect on the self-assembling of eight $[DiC_8]_n[X]$ salts in water (with X = F, $MeSO_3$, Cl, Br, NO_3, SO_4, MoO_4, and WO_4). The knowledge of anion effects on the self-aggregation is of great significance[16−24] not only for basic understanding but also for a wide range of applications such as foaming, detergency, and emulsification as well as in biology, where the effect of cationic surfactants on nucleic acids can depend on the choice of the counterion.[19,20]

Recently, we reported the relevance of dimethyldioctylammonium molybdate $[DiC_8]_2[MoO_4]$ and tungstate $[DiC_8]_2[WO_4]$.[25]

Received: February 17, 2011
Revised: August 1, 2011
Published: September 01, 2011

Table 1. Critical Aggregation Concentrations CAC_σ, CAC_κ, CAC_d, CAC_1, and CAC_2 (mM), and dimerization constant, K_d (M^{-1}), obtained for $[DiC_8]_n[X]$ at 25 °C

	tensiometry	conductivity	$[DiC_8]$-selective electrode			
[X]	CAC_σ (mM)[a]	CAC_κ (mM)[a]	CAC_d (mM)[b]	K_d (M^{-1})[c]	CAC_1 (mM)[a]	CAC_2 (mM)[a]
MoO_4^{2-}	8.0	10.1	n.s.[d]	n.s.[d]	10.4	
SO_4^{2-}	10.0	11.8	n.s.[d]	n.s.[d]	12.0	
WO_4^{2-}	8.9	10.9	n.s.[d]	n.s.[d]	10.9	
F^-	9.6	8.8	n.d.[e]	n.d.[e]	n.d.[e]	
Cl^-	12.0	32.0 (30.0)[f]	0.2	166	10.0	32.0
Br^-	19.9	21.5 (23.0)[g]	0.02	4510	20.0	
$MeSO_3^-$	15.2	20.1	0.01	9310	15.2	22.1
NO_3^-	18.6	21.1	0.003	25 980	21.8	

[a] The standard deviation is estimated at ±10%. [b] Defined as the highest concentration located on the pseudo-Nernstian part of the emf curves. [c] Calculated from eq 1. [d] Not seen. [e] Not determined because [F] is not compatible with the electrode. [f] CAC taken from refs 15, 38, and 39. [g] CAC taken from ref 40.

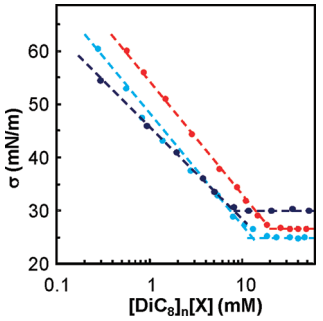

Figure 1. Surface tension (σ) plotted against $[DiC_8]_n[X]$ concentration at 25.0 °C (dark blue, $[MoO_4]$; blue, [Cl]; red, [Br]).

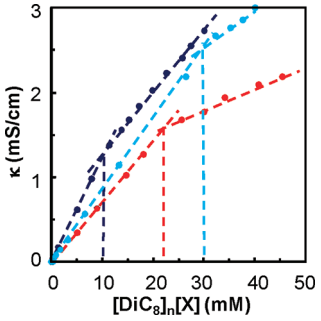

Figure 2. Specific conductivity (κ) plotted against $[DiC_8]_n[X]$ concentration at 25.0 °C (dark blue, $[MoO_4]$; blue, [Cl]; red, [Br]).

Actually, these compounds behave as "balanced catalytic surfactants", since they are able to form spontaneously three-liquid-phase microemulsion systems that can be used to perform oxidation reactions with hydrogen peroxide. It is thus important to know the self-aggregation properties of such compounds in water to anticipate their behavior in more complex water/oil systems. Generally, di-*N*-alkyldimethylammonium salts are known to form micelles, bilayers, or vesicles, even in relatively dilute solutions, depending on the hydrophobic chain length.[16−24] However, in most cases, longer alkyl chain lengths (≥10 atom carbons) are considered. In this paper, the combination of several experimental techniques (tensiometry, conductimetry and $[DiC_8]$-selective electrode) has been used to rationalize the stepwise aggregation process of $[DiC_8]$ salts as a function of the nature of the anion. The size and shape of $[DiC_8][Cl]$ and $[DiC_8]_2[MoO_4]$ aggregates has then been investigated in detail by performing dynamic light and small-angle neutron scattering (DLS and SANS, respectively) as well as molecular dynamic simulations.

RESULTS AND DISCUSSION

Self-Aggregation Properties. In this section, we report on the self-aggregation properties of eight $[DiC_8]_n[X]$ surfactants, where [X] is either a monoanion ([F], $[MeSO_3]$, [Cl], [Br], $[NO_3]$), or a dianion ($[SO_4]$, $[MoO_4]$, $[WO_4]$). Tensiometry, conductimetry, potentiometry, and DLS are used as complementary techniques to investigate the successive steps of surfactant aggregation. All results are summarized in Table 1, but for sake of clarity, only three anions ($[MoO_4]$, [Cl], [Br]) are presented in Figures 1 (tensiometry) and 2 (conductimetry), whereas five anions ($[MoO_4]$, $[MeSO_3]$, [Cl], [Br], $[NO_3]$) are shown in Figure 3 (potentiometry); and two anions ($[MoO_4]$, [Cl]), in Figure 4 (DLS).

It is noteworthy that for such a study, high purity of the surfactant is crucial, and contamination by amphiphilic impurities must be avoided. Hence, because the synthesis of the dimethyldioctyl ammonium salts is based on anion metathesis from the $[DiC_8][Br]$ salt, we have determined the residual bromide salt in each prepared salt with a [Br]-selective electrode. On the basis of a standard curve obtained with $[DiC_8][Br]$ salt, we could determine that the percentage of residual bromide does not exceed 0.1% (see the Supporting Information). In the same manner, the amount of residual dimethyloctylamine, which is obtained from the first step of the salt preparation or from Hofmann eliminations, was evaluated from gas chromatography analyses, confirming that the amine proportion is largely inferior to 0.1% (see Supporting Information). In addition to the fact that the tensiometry curves do not exhibit a dip at the cmc that reflects the presence of impurities, we can assert that all the investigated dimethyldioctylammonium salts are highly pure (>99.8%).

(i). Surface Activities. The profiles of surface tension (σ) versus log (surfactant concentration) curve are typical of soluble surfactants that adsorb at the air/water interface (Figure 1). The surface tension decreases until reaching a limiting value that does not change appreciably when the concentration is further increased. This critical concentration coincides with the surface saturation by

surfactant molecules, and it is the beginning of an aggregation process, named here CAC_σ. It is noteworthy that a "smooth" transition between 8 and 22 mM is observed for [Cl], contrary to [Br] or [MoO_4] counteranion, which exhibit a clear break at CAC_σ (Figure 1 and Table 1).

(ii). Conductivity. Specific conductivity experiments were carried out on aqueous solutions of various $[DiC_8]_n[X]$ salts. Typical plots for some [X] = [MoO_4], [Cl], and [Br] are presented in Figure 2.

It is well-known that the specific conductivity is linearly correlated to the surfactant concentration in both pre- and postaggregation regions, the slope in the preaggregation region being higher than that in the postaggregation one.[26] The break is due to the binding of some of the counterions to the aggregate and to the lower mobility of the micelles compared with the unimers (i.e., nonaggregated quaternary ammonium salt). The break point corresponds to the CAC, called here CAC_κ (Table 1).

(iii). [DiC_8]-Selective Electrode. The equilibrium electromotive force (emf) of aqueous solutions was recorded from 0.001 to 100 mM using a homemade [DiC_8]-selective electrode constructed from a pH glass electrode coated with a silicon polymer containing [DiC_8][BPh_4] as a cation exchanger.[15] Between each measurement, the electrode was washed several times with absolute ethanol to avoid any possible perturbation due to surfactant adsorption. The chemical reactivity of [F] with the silicone membrane of the electrode prevented our analysis of [DiC_8][F] by this method. Figure 3 represents the emf versus $[DiC_8]_n[X]$ concentration curves obtained for [MoO_4], [Cl], [Br], [$MeSO_3$], and [NO_3] salts (the emf curves of [WO_4] and [SO_4] salts are given in the Supporting Information).

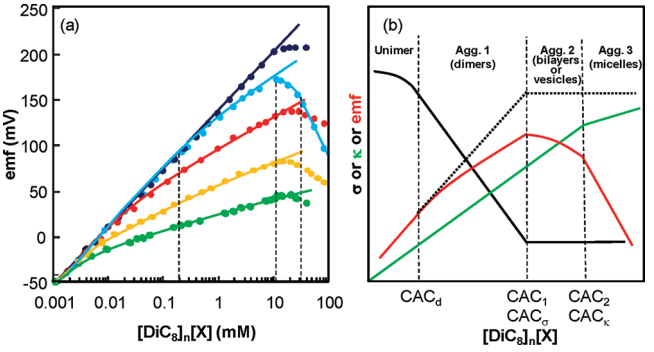

Figure 3. (a) Experimental and calculated (solid curves, see eq 1) emf plotted against $[DiC_8]_n[X]$ concentration at 25.0 °C (dark blue, [MoO_4]; blue, [Cl]; red, [Br]; orange, [$MeSO_3$]; green, [NO_3]). (b) Schematic representation of the possible surface tension, conductivity, and emf variations as a function of $[DiC_8]_n[X]$ concentration in relation to the aggregation state (N.B.: Some transitions are not necessarily observed).

The [DiC_8]-selective electrode displays a pseudo-Nernstian behavior at low concentrations, that is, the emf linearly increases with the logarithm of the surfactant concentration with a slope of 63.4 mV.[15] This value is close to that obtained for similar surfactants, such as di-*N*-decyldimethylammonium bromide ([DiC_{10}]-[Br]) (58.3 mV).[27] It is important to specify that membrane electrodes exhibit a pseudo-Nernstian behavior, that is, a linear variation with a slope that may differ from 59.2 mV, since this slope depends on (i) the nature and (ii) the charge of the ion carrier in the membrane (e.g., [DiC_8][$B(Ph)_4$]).[28,29] Thus, the value of the slope does not express the reversibility of the electrode contrary to classical Nernstian redox electrodes and does not prevent its providing accurate and reproducible measurements of the concentration of free [DiC_8] cations.

(iv). Discussion. CAC_σ, CAC_κ, CAC_d, CAC_1, CAC_2 values, and dimerization constant (K_d) determined by surface tension, conductivity, and [DiC_8]-selective electrode measurements for the eight counter anions investigated are given in Table 1.

It is clear from Figure 3a and Table 1 that the nature of the counteranion has a strong influence on the aggregation process of $[DiC_8]_n[X]$ salts.[30−37] When the anions are salting-out, that is, highly hydrated ([F], [MoO_4], [WO_4], and [SO_4]), the CAC values obtained from the three methods are close to each other: $CAC_\sigma \approx CAC_\kappa \approx CAC_1 = CAC_2$. Moreover, before this common CAC, the emf linearly increases according to the pseudo-Nernstian equation. Thus, we can confidently assume that only one type of aggregation occurs. In contrast, the behavior of monovalent anions (except [F]) is more complex. The different discontinuities observed in the emf profiles (Figure 3a) suggest the stepwise formation of different types of aggregates when the $[DiC_8]_n[X]$ concentration increases (Scheme 1).[15]

In a concentration range between CAC_d and ~10 mM, the emf clearly deviates from the expected pseudo-Nernstian line. This nonideal behavior, already observed with [DiC_8][Cl],[15] is even more pronounced when the anions are less salting-out (e.g., compare [Cl] and [NO_3].) It has been ascribed to the formation of dimers of [DiC_8] above a concentration called the CAC_d.[41−44] According to the model previously developed for the dimerization

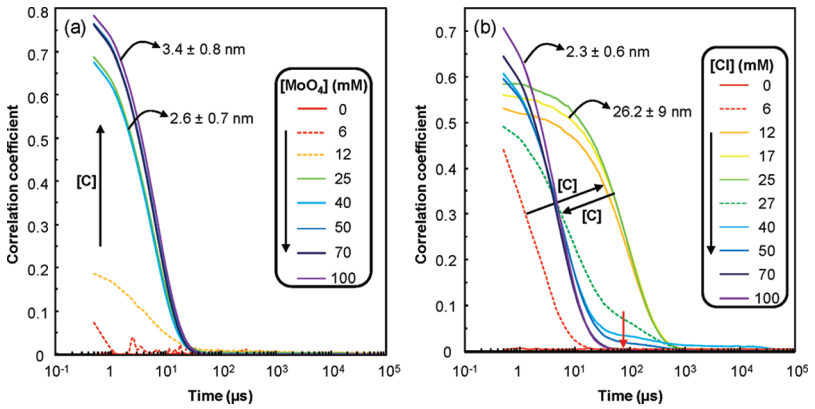

Figure 4. DLS experiments: correlation coefficient recorded at different concentrations of (a) $[DiC_8]_2[MoO_4]$ and (b) [DiC_8][Cl] (T = 25 °C and detection angle of 173°).

Scheme 1. Stepwise Self-Aggregation and Different Types of Aggregates Possibly Formed When Increasing the Concentration of $[DiC_8]_n[X]$[a]

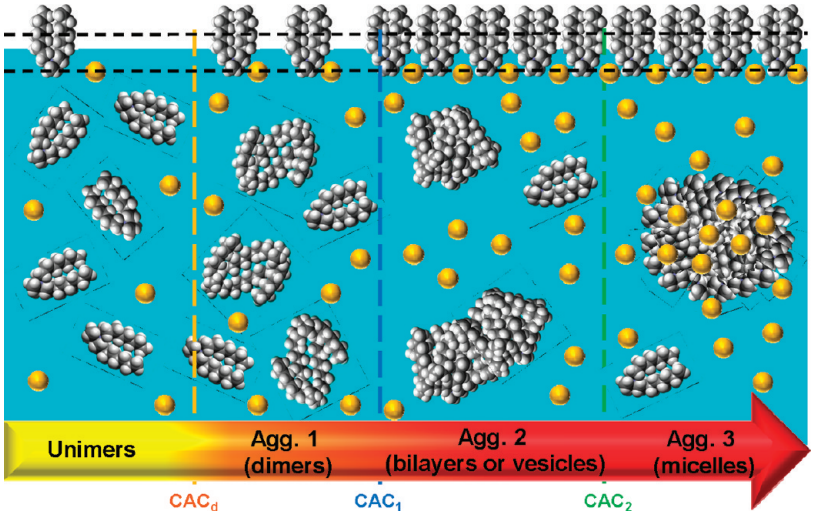

[a] N.B.: Some transitions are not necessarily observed.

equilibrium, the emf value depends on the total concentration, C_t, and the association constant, K_d, as expressed by the following equation.[15]

$$\text{emf} = 324.6 + 63.4 \times \log\left(\frac{-1 + \sqrt{1 + 8K_d C_t}}{4K_d}\right) \quad (1)$$

The experimental emf data were fitted with eq 1 to access K_d values, which are reported in Table 1. Figure 3a shows that the solid curves calculated from this model are in good agreement with the experimental data. It is noteworthy that K_d values increase a lot with the anion hydrophobicity (e.g., 166 M^{-1} for $[DiC_8][Cl]$ versus 25 980 M^{-1} for $[DiC_8][NO_3]$). In this part of the curve, emf steadily increases until a maximum value, called CAC_1, is reached, then the emf linearly decreases for most anions, except for [Cl] and $[MeSO_3]$, whose curves exhibit a smooth variation down to a second break called CAC_2, from which the emf linearly decreases, as well. In the same way, surface tension and conductometric measurements highlight the different behaviors of [Br] and $[NO_3]$ on one side and [Cl] and $[MeSO_3]$ on the other side. Indeed, the first two anions give the same CACs, whatever the method ($CAC_\sigma \approx CAC_\kappa \approx CAC_1 = CAC_2$), whereas the two others exhibit two distinct values of CAC with $CAC_\sigma \approx CAC_1$ and $CAC_\kappa \approx CAC_2$).

The difference between the CACs determined by tensiometry, conductimetry, and potentiometry observed in the case of dimethyldioctyl ammonium salts can be explained by the specificity of these methods, as reported in our previous work.[15] Surface tension is a surface measurement, whereas conductimetry and potentiometry are bulk measurements. Therefore, the surface tension decreases until surface saturation (CAC_1), even if a new equilibrium appears in the bulk due to dimerization in the meantime. When they are favored, the dimers (aggregate 1) can be seen as a reservoir of unimers that are readily available for adsorption of $[DiC_8][X]$ at the water/air interface, and therefore, the dimers will not limit adsorption. Indeed, the relaxation time, τ, for the release of unimers from the dimers into the bulk is the driving process to be considered. It can be concluded that a short relaxation time τ is important for supplying fresh unimers from the dimers to the interface. τ depends on the molecular dimerization equilibrium. On the basis of the surface tension results, the equilibrium surface tension is achieved before 60s for all concentrations investigated here (i.e., inferior to the time windows over which dynamic surface tension measurements can be made using the ring technique). Therefore, we can suppose that the diffusion process from the subsurface to the interface is the rate-controlling step, that is, τ is short; thus, no influence on the surface tension is observed. These assumptions are supported by several reported works that describe the same phenomenon for micelles.[45−48]

The break point detected by conductimetry results from an increase in the condensation of some of the counterions to the aggregate and to the lower mobility of the micelle. This phenomenon occurs at the transition (CAC_2) between aggregate 2 (bilayers or vesicles) and aggregate 3 (micelles). At last, the specific electrode is able to detect any transition between the different types of aggregates shown in Figure 3b and in Scheme 1, since it measures the concentration of free $[DiC_8]$. It is noteworthy that, in the case of $[DiC_{10}][Cl]$, which is well-known to provide only one transition from micelles to aggregates, the three methods give a similar value for the cmc from 1.2 to 1.7 mM (see Supporting Information S4), which is in good agreement with the value reported by del Burgo et al.[49]

(v). Dynamic Light Scattering. The evolution of the correlograms when increasing the concentration of $[DiC_8]_n[X]$ is very different for $[MoO_4]$ and [Cl] salts (Figure 4). Indeed, this technique has proven to be advantageous in the study of the sizes of supramolecular assemblies.[50] Typical deviating correlation functions corresponding to the formation of aggregates are obtained (Figure 4). In the case of $[MoO_4]$, no autocorrelation function could be recorded for 6 mM, whereas the signal obtained at higher concentration remains almost constant, corresponding to an aggregation size of 2.6 ± 0.7 nm for 12, 25, and 40 mM and 3.4 ± 0.8 nm for 50, 70, and 100 mM. This result is in good agreement with previous measurements; that is, no aggregates are formed below 10 mM, and a single type of small aggregates

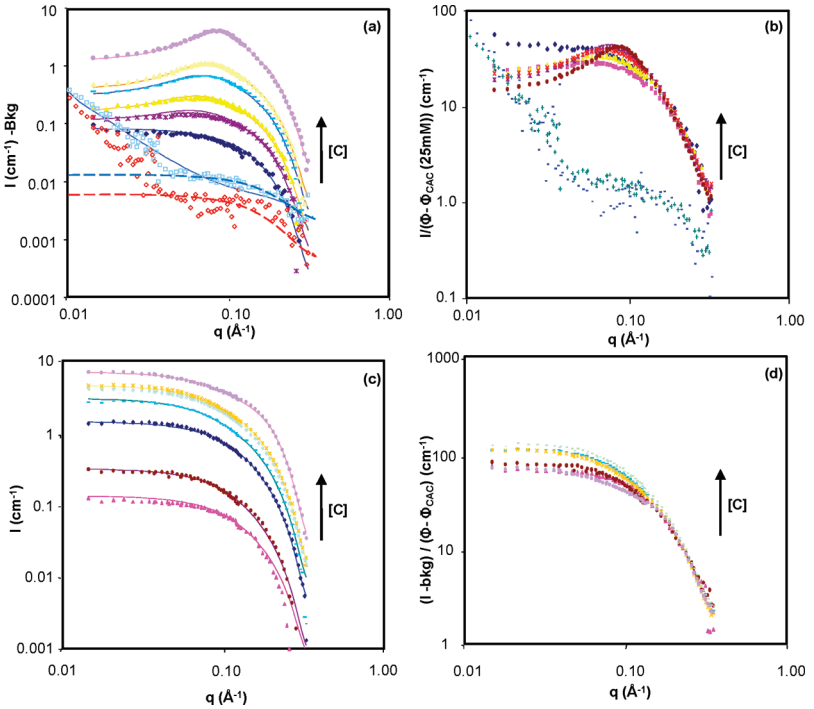

Figure 5. SANS spectra of $[DiC_8][Cl]$ (a) and $[DiC_8]_2[MoO_4]$ (c) in D_2O as a function of concentration (see Table 2). Parts b and d show the SANS spectra for $[DiC_8][Cl]$ and $[DiC_8]_2[MoO_4]$, respectively, after normalization (see text). For fit explanations, see the text.

appears above the CAC. Again, the behavior of [Cl] salt is more complex, with small aggregates formed, since 6 mM (i.e., a correlogram is obtained) is followed by a considerable increase in the size between 12 and 25 mM and, finally, an unexpected decrease in the size at very high concentration (between 40 and 100 mM). At low concentrations ($\leq$25 mM), the correlogram is typical of a sample containing large particles (26.2 $\pm$ 9 nm), but for a concentration range $\geq$40 mM, the correlation functions correspond to small aggregates (i.e., the signal decays more rapidly, and the aggregate size is assessed at 2.3 $\pm$ 0.6 nm). It is noteworthy that at 27 mM, the correlogram indicates a transition between large and small aggregates (see dark red arrow). DLS experiments confirm the unusual behavior of the [Cl] anion compared with $[MoO_4]$.

Small Angle Neutron Scattering. To confirm the unusual DLS autocorrelation functions obtained for $[DiC_8][Cl]$, the size and shape of $[DiC_8][Cl]$ and $[DiC_8]_2[MoO_4]$ aggregates were investigated further by resorting SANS experiments between 10 and 300 mM. It is noteworthy that for concentrations below 10 mM, the sensitivity of neutron scattering is not high enough to provide information on dimers.

(i). Results. SANS spectra of $[DiC_8][Cl]$ and $[DiC_8]_2[MoO_4]$ in D_2O as a function of concentration can be seen in Figure 5.

Large differences in the scattering patterns can be observed between the two surfactants. For $[DiC_8]_2[MoO_4]$, no q^{-2} dependence is observed over the range of studied concentrations, unlike $[DiC_8][Cl]$. Indeed, for $[DiC_8][Cl]$, in the low concentration regime, at 10 and 20 mM, the scattering intensities exhibit a q^{-2} dependence in the low-q region, consistent with disklike micelles, as discussed later. Similar q^{-2} dependence in the low-q region was observed in SANS measurements of a photoresponsive cationic bolaform surfactant, which indicates the formation of a bilayer structure.[51] For surfactant concentrations above 20 mM, the scattered intensity pattern is very different. This difference is likely linked to a change in the shape of the aggregates above and below $\approx$25 mM, which is the concentration region corresponding to CAC_2 observed by other techniques (see below).[15] The q^{-2} dependence is not observed anymore, and a classical scattering pattern of micelles is observed. In addition, an interaction peak is observed from 40 mM, meaning that micelles are exposed to repulsive interactions.

As for classical ionic surfactants (sodium dodecyl sulfate, SDS, or dodecyltrimethylammonium bromide, $[C_{12}][Br]$), the interaction is of electrostatic origin. For $[DiC_8]_2[MoO_4]$, no q^{-2} dependence is observed, and in comparison with $[DiC_8][Cl]$, the scattering spectra do not show any interaction peak. Consequently, micelles formed by $[DiC_8]_2[MoO_4]$ are not exposed to strong repulsive interactions. A simple phenomenological treatment to highlight changes in the aggregate types in solution is to normalize the SANS spectra (see Figure 5b and d) with the volume fraction of scattering objects, defined as $\phi_{scattered} = \phi_{total} - \phi_{CAC}$ where ϕ_{CAC} corresponds to the volume fraction at the critical aggregation concentration, taken here as $\phi_{CAC} = 0.009$ and 0.0035 and corresponding to 27 and 10 mM for $[DiC_8][Cl]$ and $[DiC_8]_2[MoO_4]$, respectively (see below).

For $[DiC_8][Cl]$, the normalization was done with ϕ_{total} instead of $\phi_{total} - \phi_{CAC}$ for the two concentrations below the CAC_2, that is, 10 and 20 mM. The difference in the curves above and below 25 mM is, indeed, much larger after normalization, confirming the different types of aggregates. Moreover, above 20 mM, the curves superimpose in the high-q regime above 0.15 $Å^{-1}$ where the main contribution to the scattered intensity is given by the form factor, the structure factor being approximated to be 1. This indicates that the shape and size of the micelles do not change in the concentration range from 30 to 300 mM. In the lower-q range, the curves are much different because of the change in the structure factor reflecting the repulsive interactions between the aggregates. Moreover, for 10 and 20 mM, the normalized curves

superimpose over the whole accessible q range, meaning that the disklike structure is the same and that no interaction occurs between the aggregates at these low concentrations.

For $[DiC_8]_2[MoO_4]$, all the curves superimpose in the high-q regime above 0.15 $Å^{-1}$ (Figure 5d). At lower q values, the differences between the curves reflect the interactions between the micelles. Hence, for $[DiC_8][Cl]$, a discoid-to-ellipsoid structure transition apparently occurs over a relatively sharp concentration range (20−30 mM). Such a phase transition as a function of surfactant concentration is relatively rare and is known so far only for mixtures of surfactants.[52] For example, this was observed for photosensitive surfactants because of the presence of two isomers of very different hydrophilic/lipophilic ratios.[53]

(ii). Fitting Procedure of the Scattered Intensity below the CAC$_2$ for [DiC$_8$][Cl]. In the high-q regime above 0.04 $Å^{-1}$, a classical signature of small scattering objects can be observed. To check if this signal could be due to the presence of dimers, observed with the ion-selective electrode, we made the approximation that $[DiC_8]$ dimers have an overall cylindrical shape (see Figure 6). Hence, a fitting procedure was performed by using a form factor of a simple cylinder ($P(Q)_{sphere}$; see eq 5) by assuming that no interaction is present at such low concentrations, then that S(Q) can be safely taken as equal to 1 (see eq 3). The scattering curves for 10 and 20 mM are well fitted with this model in the high-q regime. See solid lines in Figure 5a, for cylindrical particles of section ($R_{cyl.}$) 4.3 Å and length (L) 22.0 Å. Such a cylinder is in agreement with the molecular organization of a dimer as sketched in Figure 6.

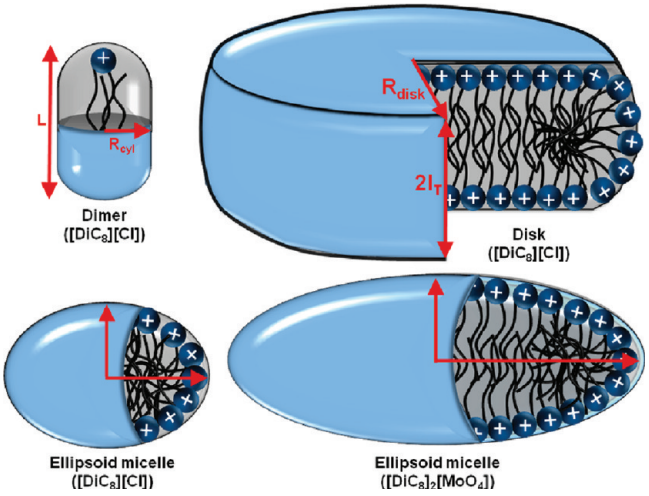

Figure 6. Schematic representation of some aggregates obtained from SANS data.

The volume of the scattering particles, $V_P = \pi R_{cyl}^2 L = 1278$ $Å^3$, is then about 2 times the molecular volume of $[DiC_8][Cl]$, $V_m = 576$ $Å^3$, meaning the scattering in the high-q regime is likely to be due to the presence of dimers. To check this hypothesis, the concentration of particles, n_P, obtained from the fit (see eq 3 and the fit results in Table 2) is analyzed further. The $[DiC_8][Cl]$ concentrations can be calculated from the fit parameter n_P by the expression $[DiC_8][Cl] = n_P \times n_{agg}$ with $n_{agg} = V_P/V_m$; 9.44 and 18.9 are found instead of the 10 and 19.9 mM obtained experimentally. Hence, the scattering in the high-q regime is due to the dimers, and most of the surfactant molecules are present in the aggregation state in this range of concentration. This means that only a small fraction of the surfactant participates in the formation of the disklike aggregates. To confirm this statement, a fit was performed on all the accessible q range by taking into account two contributions to the scattered intensity: (i) the first one from the dimer as it was done above and (ii) the second one from the disk aggregate (see eq 6).

The results of the fit for 20 mM are shown in Figure 7a (dashed line). The disk concentration and the radius of the disk are obtained from the fit $n_{disk} = 2.01 \times 10^{-9}$ disk nm^{-3} and $R_{disk} = 62.9$ nm, respectively, with the thickness of the film being fixed at $2l_T$ ($l_T = 11.6$ Å).[54] As for dimers, the $[DiC_8][Cl]$ concentration can be calculated from n_P with $[DiC_8][Cl] = n_p \times n_{agg}$ with $n_{agg} = V_P/V_m = \pi R_{Disk}^2 t/V_P = 48\,066$ and $n_p = n_{Disk}$. The $[DiC_8][Cl]$

Table 2. Fitted Parameters for the SANS Spectra for $[DiC_8][Cl]$ and $[DiC_8]_2[MoO_4]$

Guinier analysis							form and structure factors				
[C], mM	ϕ, × 10^2	ϕ−ϕ$_{CAC}$, × 10^2	R_g, Å	I_0, × 10^2 cm^{-1}	n_{agg}	R (L), Å	ν	Z_{eff}	n_{Pfit}, × 10^5 nm^{-3}	n_P, × 10^5 nm^{-3}	ϕ$_{S(Q)}$, × 10^2
						[DiC_8][Cl]					
10	0.35					4.3 (22)			235		
19.9	0.69					4.3 (22)			470		
29.9	1.04	0.17	11.0	6.51	16.6	12.9	1.73		7.94	10.8	
39.9	1.39	0.52	11.0	17.48	13.9	12.9	1.73	9	20.0	33.1	3.8
49.9	1.73	0.87	11.0	33.50	15.8	12.9	1.73	9	36.4	55.3	5.5
74.8	2.60	1.73	11.2	70.50	16.5	12.9	1.73	9	84.7	110.7	7.5
99.7	3.46	2.59	11.2	100.3	15.7	12.9	1.73	9	137	166.0	10.0
300	10.4	9.55	11.2	320.5	13.5	12.9	1.73	6	510	611.4	15.0
						[DiC_8]$_2$[MoO_4]					
15	0.52	0.17	11.0	11.0	25.9	12.7	2.3		9.05	11.4	0.52
21	0.73	0.38	11.0	25.0	26.6	12.7	2.3		21.8	24.8	0.73
50	1.74	1.39	11.0	86.0	25.0	12.7	2.3		108	96.3	1.74
80	2.78	2.43	11.0	147.0	24.4	12.7	2.9		159	173	2.78
103	3.58	3.23	11.0	230.0	28.7	12.7	2.9		240	195	3.58
130	4.51	4.16	11.0	265.0	25.6	12.7	2.9		282	282	4.51
300	10.4	10.1	11.0	655.0	26.2	12.7	2.9		678	667	10.4

dx.doi.org/10.1021/jp201590x |J. Phys. Chem. B 2011, 115, 11619–11630

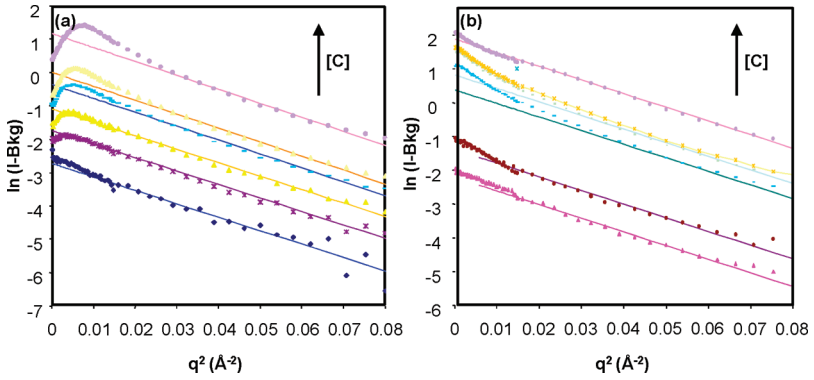

Figure 7. Guinier fits of the SANS spectra for (a) $[DiC_8][Cl]$ and (b) $[DiC_8]_2[MoO_4]$ in D_2O as a function of concentration.

concentration forming disks is then equal to 0.16 mM, in comparison with the total concentration of 19.9 mM. It is noteworthy that if the same calculation is made by performing a fit using a form factor of a shell (vesicle) instead of a disk of thickness $2l_T$, corresponding to a bilayer, and of radius $R_{vesicle}$ = 102.5 nm, the conclusions are the same. Hence, the precise structure of the large aggregate, vesicle or disk, cannot be resolved from the present results. It is also important to note that because no plateau is observed in the accessible low-q range, consequently, the radius values that are given represent minimal values. Moreover, only ~1% of the surfactant participates in the formation of the large aggregate.

(iii). Guinier Analysis above CAC_1 for $[DiC_8]_2[MoO_4]$ and CAC_2 for $[DiC_8][Cl]$. The Guinier plots for $[DiC_8]_2[MoO_4]$ and $[DiC_8][Cl]$ at different surfactant concentrations above CAC_1 and CAC_2, respectively, are shown in Figure 7.

Radii of gyration values, R_g, extracted from the slopes according to eq 2 are ~ 11 Å for both surfactant systems (see in Table 2). This value is comparable to the tail length of the surfactant. Hence, as was concluded above while discussing the scattering spectra normalized by the volume fraction, no substantial change in the size of the micelles is observed beyond the CACs and until 300 mM. Such an evolution is not usual as compared with classical ionic surfactants such as SDS and $[C_{12}][Br]$. For these latter, surfactant micelles exhibit an abrupt increase in R_g with increasing surfactant concentration, consistent with micelle elongation as the surfactant concentration increases beyond the CAC. The increase in the scattering intensity at zero angle, $I(0)$, can be used to estimate the number of surfactant molecules per micelles, that is, the aggregation number n_{agg}, through the expression

$$I(0) = \phi V_P \Delta\rho^2 = (C - CAC) \times N_A V_m^2 n_{agg} \Delta\rho^2 \qquad (2)$$

where N_A is Avogadro's number, $\phi = n_P V_P$ is the micelle volume fraction, $n_P = (C - CAC)N_A/n_{agg}$ is the micelle number density and $V_P = n_{agg}V_m$ is the micelle volume. The molecular volume of $[DiC_8][Cl]$ was estimated at 576 $Å^3$, assuming a density of 0.881 g mL^{-1}. The n_{agg} values for $[DiC_8][Cl]$ and $[DiC_8]_2[MoO_4]$, around 15 and 26, respectively (see Table 2), do not change notably as a function of concentration, confirming that the micelles do not grow significantly when the concentration increases. The higher n_{agg} values obtained for $[DiC_8]_2[MoO_4]$ may be due to a change in the length of the aggregate, which is not detectable by the R_g values determined by the Guinier's treatment in the q range studied. To get a better insight into the micellar structure, the scattering intensity spectra were fitted by using standard models.

(iv). Fitting Procedure of the Scattered Intensity above CAC_1 for $[DiC_8]_2[MoO_4]$ and CAC_2 for $[DiC_8][Cl]$. In the case of $[DiC_8][Cl]$, the micellar structure was investigated by fitting the SANS data using a biaxial ellipsoid form factor[55] combined with a structure factor accounting for electrostatic repulsions. Considering the remark of Glatter et al.[56] that in such a fitting procedure, the same structure factor can be obtained from different sets of parameters ϕ, Z_{eff}, and d, choice was made to keep the diameter and Z_{eff} constant. The effective diameter of the ellipsoid is given by the relation $d = 2(\nu R^3)^{1/3}$ where R, the radius of the ellipsoid, is a fitting parameter. Z_{eff} was found to give the best fits at a value of 9, except at 300 mM, where a value of 6 was more suitable. This difference is likely to be linked to the very high surfactant concentration where electrostatic interactions become more important. The disadvantage of the present method is that the volume fraction obtained from the fit ($\phi_{S(Q)}$ in Table 2) is overestimated compared with the effective volume fraction of the scattering objects calculated as $\phi - \phi_{CAC}$. On the other hand, the advantage of this fitting procedure is that the concentration of particles can be obtained directly from the fit (n_{Pfit} in Table 2) and compared with n_P obtained from the relation $n_P = (\phi - \phi_{CAC})/V_P$ where V_P is defined as $V_P = 4/3\pi R^3\nu$ = 15.62 nm^3 and $\phi - \phi_{CAC}$ is estimated from CACs value (see below) and total volume fraction. Here, n_{Pfit} represents between 60 and 80% of n_P, which is quite reasonable, providing an independent check on the quality of the fits.

In other studies, the scattering length density difference ($\Delta\rho$) is chosen as a fitting parameter, and the values of micelle charge and volume fraction are in that case considered as effective parameters.[53] In the present study, $\Delta\rho$ is taken as constant because it can be calculated with good confidence from molecular properties. Moreover, to improve the reliability of the fit, the fitting procedure was done simultaneously for all the concentrations studied with the radius of the biaxial ellipsoid, R, and the ellipticity factor, ν, taken as global parameters; that is, R and ν are fitting parameters that are kept similar for all the concentrations. The results of the fits shown in Table 2 indicate that (1) the value obtained for R is approximately equal to the tail length of $[DiC_8][Cl]$ in a fully extended conformation, l_T = 11.6 Å, as expected; and (2) ν is not high (<2), showing a slight ellipticity of the micelles. Hence, the R_g values obtained from the Guinier's treatement correspond to the section of the elliptical micelles. As for the Guinier analysis, the aggregation number, n_{agg}, can be estimated from the volume of the particle ($V_P = 4/3\pi R^3\nu$) and by considering $V_P = n_{agg}V_m$. This calculation gives n_{agg} = 27, which is

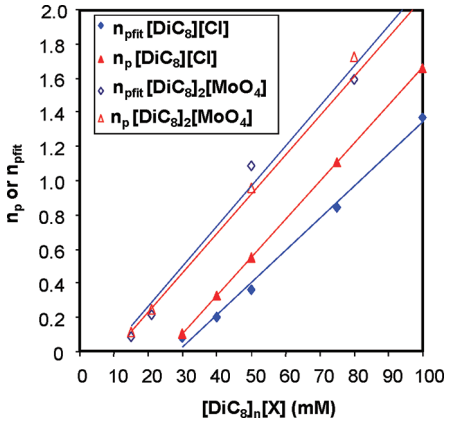

Figure 8. n_P (diamond) and n_{Pfit} (triangle) as a function of surfactant concentration for $[DiC_8][Cl]$ (solid symbols) and $[DiC_8]_2[MoO_4]$ (open symbols).

in agreement with, although larger than, the values determined from the Guinier analysis. This difference is generally explained by the presence of the diffuse counterion region, typically of 3−5 Å thickness, surrounding the micelles that gives rise to electrostatic repulsions and, hence, contributes somewhat to the fitted radii, giving an estimate of V_P.[52] Plotting n_P and n_{Pfit} as a function of surfactant concentration gives linear relations (Figure 8).

From these linear expressions, the CAC (i.e. when the aggregates start forming) is extrapolated at n_P or $n_{Pfit} = 0$, and CAC is found to be 25.1 and 28.5 mM, respectively. For the calculation of $\phi - \phi_{CAC}$, the average value will be taken as CAC = 27 mM. This CAC value corresponds to CAC_2 (around 30 mM).[15] Concerning CAC_1, which is supposed to represent the transition from dimers to discoid micelles, it cannot be accessible by neutron scattering because the sensitivity is not high enough in the low range concentration below 10 mM.

For $[DiC_8]_2[MoO_4]$, a similar fitting procedure was used. Nevertheless, because no interaction peak is observed in the studied concentration range with $[DiC_8]_2[MoO_4]$, a simple hard-sphere structure factor was used. In general, $S(q)$ for a hard sphere system does not introduce very sharp features into the scattering pattern unless one goes to very high concentrations. In the fitting procedure, the effective hard sphere radius, R_{HS}, was set as equal to the radius used in the form factor, which is a global fitting parameter (i.e. a parameter fixed for all concentrations), and the volume fraction $\phi_{S(Q)}$ was calculated from the sample compositions. As for $[DiC_8][Cl]$, the results of the fits indicate that the value obtained for R is approximately equal to the surfactant tail length. Because it was not possible to fit ν simultaneously for all concentrations, the set of concentrations was divided into two parts fitted with two distinct ν parameters. The ν values obtained are 2.3 and 2.9, respectively, for the low concentrations (15−50 mM) and for the high concentrations (80−300 mM). Hence, the ellipticity of the $[DiC_8]_2[MoO_4]$ micelles is higher than for $[DiC_8][Cl]$ micelles and shows a slight tendency to increase at higher surfactant concentrations.

To explain the effect of anion on the aggregate structure, we consider the specificity of ion interactions in solution to be dependent on both the cation and the counteranion.[57] Collins defined the tendency of ions to spontaneously pair in aqueous solutions, predicting strong interactions and ion-pairing between salting-in ions of similar size and opposite charge, and lack of interaction between salting-in and salting-out ions.[58,59] Vlachy et al. suggested extending the above concept from interactions between ions to interactions between ions and surfactant headgroups.[60] In this context, the ammonium headgroup of $[DiC_8]$ is a salting-in cation, strongly interacting with large salting-in anions, thereby releasing weakly bound water, efficiently screening electrostatic interactions, decreasing the headgroup surface area, and increasing the packing parameter. This promotes change in the ellipticity of the aggregates. As for $[DiC_8][Cl]$, the CAC can be evaluated from Figure 8. CAC is found to be 9.6 and 8.8 mM, which corresponds to a CAC_2 (around 10 mM) obtained by the other techniques such as conductimetry (10.1 mM), selective electrode (10.4 mM), or tensiometry (8 mM).[15] This good agreement validates the model we used for the fitting of the SANS spectra.

The SANS spectra for $[DiC_8]_2[SO_4]$ and $[DiC_8]_2[WO_4]$ at 100 mM were also collected and show only a slight difference compared with the spectrum of $[DiC_8]_2[MoO_4]$ (see the Supporting Information, Figure S5). The SANS curves for these three surfactants overlap in the high-q regime, meaning that the shape and size ($P(q)$) of the micelles do not depend on the type of the divalent counterion. The slight difference observed in the scattering intensity in the low-q regime is due to different repulsive interactions between micelles ($S(q)$) in the following order according to the strength of the repulsions: $[SO_4] > [WO_4] > [MoO_4]$. This discrepancy may be attributed to the effective charge of the micelle, which is a direct consequence of the binding of the counterion to the micelle, with $[MoO_4]$ being the less bound counterion.

Molecular Dynamics. To support our conclusions on the structure formed by $[DiC_8]$ salts, molecular dynamic (MD) simulations of aggregates in aqueous solution were carried out in a cubic simulation box with periodic boundary conditions in all directions (Figure 9). Several 1 000 ps runs were performed with different numbers of unimers with different initial relative orientations and various anions. In most cases, $[DiC_8][Cl]$ and $[DiC_8]_2[MoO_4]$ molecules form ellipsoid micelles within the first 100 ps of the simulation run and remain in a stable position.

Table 3 summarizes the information obtained on the aggregate structures for $[DiC_8]$ salts in aqueous solutions by the various techniques presented above. It appears that all the structures obtained from SANS and MD are in perfect accordance on the ellipsoidal nature of aggregates form by $[Cl]$ and $[MoO_4]$. For $[DiC_8][Cl]$, on the basis of dimer hypothesis due to hydrophobic interaction between the alkyl tails between two molecules, we suppose that dimerization occurs at concentrations below CAC_1 (10 mM). At surface saturation, the bulk is probably rich in dimers that interact to form more and more complex aggregates (tetramers, hexamers, octamers, etc.).[15] However, we have detected that $[DiC_8][Cl]$ molecules form discoidal micelles, probably resulting from the juxtaposition of dimers. This structure is destroyed between 20 and 30 mM to form a new ellipsoidal structure. The associated transitions are strongly affected by the nature of the counterion: for $[DiC_8]$-$[MoO_4]$ and $[DiC_8][Cl]$, ellipsoidal aggregates are finally obtained, but the mechanism (i.e., transitions) is very different.

Comparing the results obtained for dimethyldioctylammonium $[DiC_8]$ with those described in the literature for trimethyloctylammonium $[C_8]$ cations is very instructive. In fact, the $[C_8]$ cations can also be considered as a borderline case between hydrotrope and surfactant. To our knowledge, there is no report in the literature dealing with dimerization of $[C_8]$ cations in

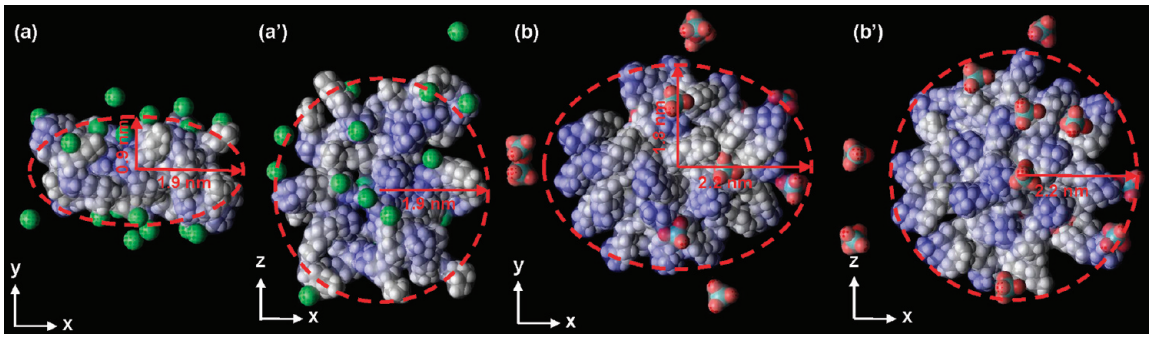

Figure 9. Final MD snapshots (1 000 ps) in water of (a) $[DiC_8][Cl]$, (a′) $[DiC_8][Cl]$ down view, (b) $[DiC_8]_2[MoO_4]$, and (b′) $[DiC_8]_2[MoO_4]$ down view. Water molecules have been removed for clarity.

Table 3. Information Obtained on the Aggregate Structure and Size for $[DiC_8]_n[X]$ Aqueous Solutions by Various Techniques at 25.0 °C

	$[DiC_8][Cl]$			
	<10 mM	10−30 mM	>30 mM	$[DiC_8]_2[MoO_4]$, 10−100 mM
		Neutron Diffusion		
structures	n.d.	discoid micelles	ellipsoid micelles	ellipsoid micelles
n_{agg}	n.d.	n.d.	±15	±26
size (nm)	n.d.	62.9 and 2.3	1.3; ν = 1.7	1.3; ν = 2.3−2.9
		DLS		
structures[a]	aggregates	discoid micelles	small aggregates	small aggregates
size (nm)[b]	n.d.	26.2 ± 9	2.3 ± 0.6	2.6−3.4 ± 0.3
		MD		
structures	dimers	discoid micelles[c]	ellipsoid micelles	ellipsoid micelles
n_{agg}	2	n.d.	18	26
size (nm)	0.9 × 0.7 × 0.4	n.d.	0.9, 1.9 ± 0.2	1.8, 2.2 ± 0.3

[a] Based on the DLS autocorrelation function. [b] Based on the distribution function calculated from the DLS autocorrelation function with a spherical hypothesis. [c] Bilayers formed by the juxtaposition of dimers.

aqueous solution. However, Gharibi et al. have reported, from emf measurements, that dimerization is observed for longer homologous cations (e.g., $[C_{10}]$, $[C_{12}]$, $[C_{14}]$, and $[C_{16}][Br]$), but the dimerization constants are very weak (<2 M^{-1}).[41] The authors also suggest the formation of trimers, but the constants remain relatively low (≈90 M^{-1} for the decyl chain). Hence, a single alkyl tail brings a low hydrophobic effect, which leads to a small dimerization constant contrary to two-tailed quaternary ammonium for which the dimerization process is notably favored. Moreover, the CAC of $[C_8][Br]$ is very high (around 220−290 mM),[61−65] and above the CAC, spherical micelles are formed.[66,67] This shape has been confirmed by molecular dynamics for $[C_8][Cl]$.[68] On the basis of these considerations, we can suppose that the two octyl tails of $[DiC_8]$ cations are necessary to obtain (1) a true dimerization that excludes trimers and (2) a decrease in the CAC (220−290 versus 10 mmol/L from one to two alkyl chains), both effects resulting in the observation of a transition between discoidal (or vesicular) and ellipsoidal aggregates.

This transition can be attributed to significant changes in the interfacial water and counterion concentrations. Indeed, a careful look at the conductivity results shows that counterions are bound to the aggregates only at the transition (e.g., around 30 mM for the chloride anion): that is, dimers are totally hydrated as the first large aggregate is observed below 30 mM. At 30 mM, the condensation of chloride to aggregates results in a shape transition. It is noteworthy that, depending on the anion charge, size and polarizability, the transition is allowed or not. This observation is in agreement with the results obtained by Romsted,[31] who has reported that the changes in interfacial water and counterion concentrations are observed during structural transitions. Specific ion effects on aggregate transitions of cationic surfactants are interpreted in terms of the strengths of headgroup, counterion pairing, and ion hydration. In other words, the formation of ion contact pairs at the aggregate/water interface results in a less hydrated shell than free ions. The excess water is released into the bulk; that is, the entropy of the system as a whole increases similarly to the hydrophobic effect. Therefore, there is a difference in interaction energies between anions and cations with each other and with their hydration shells. The water or ion effect can be invoked in the transition mechanism: the nature of counter anions (e.g., their charges, their hydration, etc.) and the competing effect of water in the aggregate/water interface have a significant contribution on the aggregate shape.

CONCLUSION

We have reported here convergent evidence for various self-aggregations of $[DiC_8]$ salts in aqueous solution, depending on

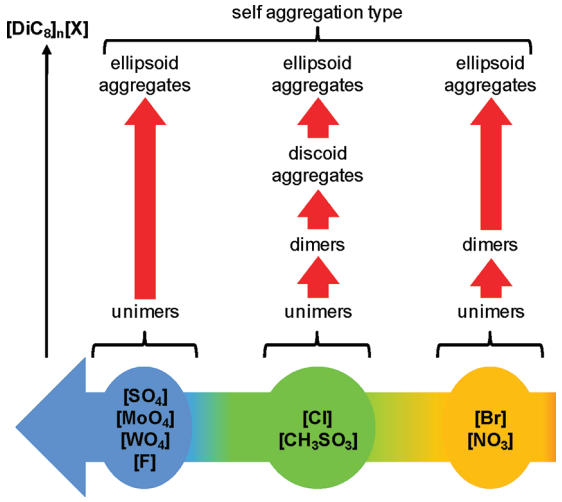

Figure 10. Proposed self-aggregations of $[DiC_8]$ in water as a function of the $[DiC_8]_n[X]$ concentration.

the hydrophilicity of the counterions as illustrated in Figure 10. Three cases could be highlighted: (i) for salting-out anions, the ordinary aggregation of $[DiC_8]_n[X]$ (with [X] = [F], $[MoO_4]$, $[WO_4]$, and $[SO_4]$) into micelles occurs at a specific concentration; (ii) for salting-in anions, the aggregation of $[DiC_8]_n[X]$ (with [X] = [Br] and $[NO_3]$) also occurs at a specific concentration, but below this concentration, some $[DiC_8]_n[X]$ salts form dimers; and (iii) for $[DiC_8]_n[X]$ with intermediate anions ([X] = [Cl] and $[MeSO_3]$), dimers also form below the surface saturation, followed by two successive self-assemblies to form micelle-like aggregates.[15] These self-aggregation processes (dimers and micelle-like aggregates) are driven by the hydrophobic effect similar to the one of the classical micellization process.

Thus, four structural features of $[DiC_8]_n[X]$ can be pointed out to account for the aggregation behavior: (i) two alkyl chains favors the dimerization through hydrophobic interactions, (ii) two relatively short chains delay the more conventional micellization phenomenon, that is, the observation window of the self-aggregation phenomenon is wider; (iii) the high hydrophilicity of the counteranion does not favor dimerization (i.e., K_d decreases); and (iv) the intermediate anion "hydrophobicity" widens the "bilayer" window. As reported in the recent publication of Manet et al., the results obtained here provide new insight into understanding the effect of anions on the delicate balance of forces controlling the aggregate morphology and the solution properties of the cationic surfactant.[69] The aggregate morphology and solution properties are very important, and ion pairing cannot be accurately described using one single parameter; rather, it requires a whole set of parameters—hydrophilicity, steric effect, valency—that may lead to very different self-aggregation behavior. SANS, DLS, and MD experiments, performed on $[DiC_8][Cl]$ and $[DiC_8]_2[MoO_4]$, strongly suggest that final aggregates are ellipsoidal. Moreover, our results confirm the two types of aggregation of $[DiC_8][Cl]$—(i) discoid and (ii) ellipsoid aggregates—and do not exclude the formation of dimers. Concerning its aggregation property, dimethyl-di-*N*-octylammonium salts $[DiC_8][X]$ present a dual behavior, depending on the anion [X] starting from a stepwise association, like hydrotropes, followed by a collective association, like surfactants.

EXPERIMENTAL SECTION

SANS Methods. The SANS data were analyzed using a range of complementary techniques, including Guinier analysis, dilution laws, and form-factor/structure-factor modeling. From the Guinier approximation,[70] the scattering intensity $I(Q)$ is given by eq 3.

$$I(q) = I(0)\exp(-q^2R_g/3) + I_b \quad (3)$$

where $I(0)$ is the extrapolated intensity at $q = 0$, R_g is the radius of gyration, and I_b is the background scattering intensity (i.e., incoherent scattering). Thus, the radius of gyration can be determined from the slope of a plot of $\ln(I(q))$ versus q^2, typically in the region where $qR \leq 1.3$. In the case of charged micelles, the structure factor influences the scattering in the low-q Guinier regime, complicating the Guinier analysis for such systems (discussed below). The SANS intensity $I(q)$ data were fit to eq 4:

$$I(q) = n_P V_P^2 \Delta\rho^2 P(q) S(q) + I_b \quad (4)$$

where n_P is the particle concentration, V_P is the volume of an individual particle (for example, a micelle), and $P(q)$ and $S(q)$ are the form and structure factors respectively. The particle concentration can be related to the volume fraction of the particles, ϕ, by $n_P = \phi/V_P$. The neutron scattering length density difference, $\Delta\rho$, between the surfactant and D_2O solvent can be estimated from the known value for D_2O (6.37×10^{10} cm^{-2}) and the calculated value for $[DiC_8][Cl]$ (1.18×10^{10} cm^{-2}) obtained from the density estimated by Chemsketch. Thus, $\Delta\rho = 6.56 \times 10^{10}$ cm^{-2}. It was checked that the presence of dimers in D_2O does not significantly change $\Delta\rho$ below 0.1% so that it could be neglected in the calculation of $\Delta\rho$. Different form factors were employed, depending on the surfactant concentration. For 10 and 20 mM, the form factor of a cylinder was employed to fit the dimer. In this case, the scattered intensity of the cylinder is expressed as

$$I_{cyl}(q) = n_{cyl}16(\pi R_{cyl}^2 L)^2 \Delta\rho^2 \int_0^1 \left(\frac{J_1\left(qR_{cyl}\sqrt{1-x^2}\right)\sin(qLx/2)}{q^2R_{cyl}\sqrt{1-x^2}Lx} \right) dx \quad (5)$$

where R_{cyl} and L are the radius of the cylinder and its length, respectively, and J_1 is the first-order Bessel function.

For 20 mM, an additional contribution of large particles, observed in the low-q regime as a q^{-2} dependence as a function of the wave vector, was taken into account by using a form factor of the circular disk. In that case, the scattered intensity was simply expressed by the sum of two contributions from the unimers and from the disks:[71]

$$I(q) = I_{cyl} + n_{Disk} V_P^2 \Delta\rho^2 P_{Disc}(q) + I_b \quad (6)$$

with

$$P_{Disc}(q) = 4\int_0^1 \frac{J_1^2\left[qR\sqrt{1-x^2}\right]}{\left[qR\sqrt{1-x^2}\right]} \times \frac{\sin^2(qLx/2)}{(qLx/2)^2} dx \quad (7)$$

For concentrations above 20 mM, the normalized form factor for a biaxial ellipsoid[72] (see eq 7) with two equal semiaxis R's and a

semiprincipal axis νR and volume $V_P = (4/3)\pi R^3\nu$ were used.[73]

$$P_{\text{Ellipsoid}}(q) = \int_0^{\pi/2} {F_1}^2\left[q, R\sqrt{\upsilon^2 \cos^2\theta + \sin^2\theta}\right] d\theta \quad (8)$$

For $[DiC_8][Cl]$, the structure factor, $S(q)$, was based on a mean spherical approximation accounting for electrostatic repulsions[74,75] and accurately describes the interactions for a wide range of charged micelles.[76−78] At low surfactant concentrations, where only unimers or dimers with very diluted micelles (i.e. $[DiC_8][Cl] \leq 30$ mM) are present, the structure factors can be approximated to 1 with good confidence. For $[DiC_8][Cl] > 30$ mM, the structure factor was simply combined with the biaxial ellipse form factor by a monodisperse approach. This structure factor is based on fitted parameters for the micelle: effective particle charge $|Z_{\text{eff}}|$, diameter, and volume fraction, along with input values for the temperature, monovalent salt concentration (set equal to the surfactant CAC = 27 mM), and solvent dielectric constant being 77.9 for D_2O. For $[DiC_8]_2[MoO_4]$, the structure factor could be well described by a hard sphere model for which an analytical expression for $S(q)$ exists in the Percus−Yevick approximation, which has been shown to be reliable for many systems.[79] This structure factor depends then on two parameters: the effective hard sphere diameter, R_{HS}, and the volume fraction, ϕ. The fits were performed using the data analysis software Sasfit 0.92.3.

■ ASSOCIATED CONTENT

Supporting Information. Experimental data and procedures. This material is available free of charge via the Internet at http://pubs.acs.org.

■ AUTHOR INFORMATION

Corresponding Author
*E-mail: veronique.rataj@univ-lille1.fr.

■ ACKNOWLEDGMENT

We are grateful to the Fonds Européens de Développement Régional (FEDER) and to the ANR (Project ANR-10-CD2I-01) for financial supports.

■ REFERENCES

(1) Cragg, P. J. *Supramolecular Chemistry: From Biological Inspiration to Biomedical Applications*; Springer: New York, 2010.
(2) Steed, J. W.; Atwood, J. L. *Supramolecular Chemistry*, 2nd ed.; Wiley: Chichester, 2009.
(3) Steed, J. W.; Turner, D. R.; Wallace, K. J. *Core Concepts in Supramolecular Chemistry and Nanochemistry*; John Wiley & Sons: Chichester, 2007.
(4) Ariga, K.; Kunitake, T. *Supramolecular Chemistry: Fundamentals and Application*; Springer: New York, 2006.
(5) Leclercq, L.; Schmitzer, A. R. *J. Phys. Chem. B* **2008**, *112*, 11064–11070.
(6) Borovkov, V. V.; Hembury, G. A.; Inoue, Y. *Angew. Chem., Int. Ed.* **2003**, *42*, 5310–5314.
(7) Xu, H.; Stampp, S. P.; Rudkevich, D. M. *Org. Lett.* **2003**, *5*, 4583–4586.
(8) Cui, Y. *Int. J. Pharm.* **2010**, *397*, 36–43.
(9) Bauduin, P.; Renoncourt, A.; Kopf, A.; Touraud, D.; Kunz., W. *Langmuir* **2005**, *21*, 6769–6775.
(10) Cuil, Y.; Xing, C.; Ran, Y. *J. Pharm. Sci.* **2010**, *99*, 3048–3059.
(11) Hodgdona, T. K.; Kaler, E. W. *Curr. Opin. Colloid Interface Sci.* **2007**, *12*, 121–128.
(12) Da Silva, R. C.; Spitzer, M.; Da Silva, L. H. M.; Loh, W. *Thermochim. Acta* **1999**, *328*, 161–167.
(13) Srinivas, V.; Rodley, G. A.; Ravikumar, K.; Robinson, W. T.; Turnbull, M. M.; Balasubramanian, D. *Langmuir* **1997**, *13*, 3235–3239.
(14) Balasubramanian, D.; Srinivas, V.; Gaikar, V. G.; Sharma, M. M. *J. Phys. Chem.* **1989**, *93*, 3865–3870.
(15) Leclercq, L.; Nardello-Rataj, V.; Turmine, M.; Azaroual, N.; Aubry, J.-M. *Langmuir* **2010**, *26*, 1716–1723.
(16) Jusufi, A.; Hynninen, A.-P.; Haataja, M.; Panagiotopoulos, A. Z. *J. Phys. Chem. B* **2009**, *113*, 6314–6320.
(17) Maiti, K.; Mitra, D.; Guha, S.; Moulik, S. P. *J. Mol. Liq.* **2009**, *146*, 44–51.
(18) Pinazo, A.; Pérez, L.; Lozano, M.; Angelet, M.; Infante, M. R.; Vinardell, M. P.; Pons, R. *J. Phys. Chem. B* **2008**, *112*, 8578–8585.
(19) Pardin, C.; Leclercq, L.; Schmitzer, A. R. *Chem.—Eur. J.* **2010**, *16*, 4686–4692.
(20) Jiang, N.; Peixun, L.; Wang, Y.; Yan, H.; Thomas, R. K. *J. Phys. Chem. B* **2004**, *108*, 15385–15391.
(21) Jiang, N.; Peixun, L.; Wang, Y.; Yan, H.; Thomas, R. K. *J. Colloid Interface Sci.* **2005**, *286*, 755–760.
(22) McGillivray, D. J.; Thomas, R. K. *Langmuir* **2003**, *19*, 7719–7726.
(23) Marques, E. F.; Regev, O.; Khan, A.; Lindman, B. *Adv. Colloid Interface Sci.* **2003**, *100−102*, 83–104.
(24) Ono, Y.; Kawasaki, H.; Annaka, M.; Maeda, H. *J. Colloid Interface Sci.* **2005**, *287*, 685–693.
(25) Nardello-Rataj, V.; Caron, L.; Borde, C.; Aubry, J.-M. *J. Am. Chem. Soc.* **2008**, *130*, 14914–14915.
(26) Rosen, M. J. *Surfactants and Interfacial Phenomena*, 3rd ed.; Wiley-Interscience: New York, 2004.
(27) Funasaki, N.; Neya, S. *Langmuir* **2000**, *16*, 5343–5346.
(28) Sirieix-Plénet, J.; Turmine, M.; Letellier, P. *Talanta* **2003**, *60*, 1071–1078.
(29) Peyre, V.; Baillet, S.; Letellier, P. *Anal. Chem.* **2000**, *72*, 2377–2382.
(30) Leontidis, E. *Curr. Opin. Colloid Interface Sci.* **2002**, *7*, 81–91.
(31) Romsted, L. *Langmuir* **1997**, *23*, 414–424.
(32) Ninham, B. W.; Hashimoto, S.; Thomas, J. K. *J. Colloid Interface Sci.* **1983**, *95*, 594–596.
(33) Nyden, M.; Söderman, O.; Hansson, P. *Langmuir* **2001**, *17*, 6794–6803.
(34) Livney, Y. D.; Portnaya1, I.; Faupin, B.; Ramon, O.; Cohen, Y.; Cogan, U.; Mizrahi, S. *J. Polym. Sci., Part B* **2003**, *41*, 508–519.
(35) Berr, S.; Jones, R. R. M.; Johnson, J. S., Jr. *J. Phys. Chem.* **1992**, *96*, 5611–5614.
(36) Magid, L. J.; Han, Z.; Warr, G.; Cassidy, M. A.; Butler, P. D.; Hamilton, W. A. *J. Phys. Chem. B* **1997**, *101*, 7919–7927.
(37) Kunz, W. *Specific Ion Effects*; World Scientific Publishing: London, 2010.
(38) Lang, J. *J. Phys. Chem.* **1982**, *86*, 992–998.
(39) Milioto, S.; Bakshi, M. S.; Crisantino, R.; De Lisi, R. *J. Colloid Interface Sci.* **1993**, *159*, 354–365.
(40) Hiramatsu, K.; Kameyama, K.; Ishiguro, R.; Mori, M.; Hayase, H. *Bull. Chem. Soc. Jpn.* **2003**, *76*, 1903–1910.
(41) Gharibi, H.; Palepu, R.; Bloor, D. M.; Hall, D. G.; Wyn-Jones, E. *Langmuir* **1992**, *8*, 782–787.
(42) Gillitt, N. D.; Savelli, G.; Bunton, C. A. *Langmuir* **2006**, *22*, 5570–5571.
(43) Zimmels, Y.; Lin, I. J. *Colloid Polym. Sci.* **1974**, *252*, 594–612.
(44) van Voorst Vader, F. *Trans. Faraday Soc.* **1961**, *57*, 110–115.
(45) Aniannson, E. A. G.; Wall, S. N. *J. Phys. Chem.* **1974**, *78*, 1024–1030.
(46) Aniannson, E .A. G.; Wall, S. N. *J. Phys. Chem.* **1975**, *79*, 857–858.
(47) Aniannson, E. A. G.; Wall, S. N.; Almgren, M.; Hoffman, H.; Kielman, I.; Ulbritcht, W.; Zana, R.; Lang, J.; Tondre, C. *J. Phys. Chem.* **1976**, *80*, 905–922.

(48) Johner, A.; Joanny, J. F. *Macromolecules* **1990**, *23*, 5299–5311.
(49) del Burgo, P.; Aicart, E.; Junquera, E. *Colloids Surf. A* **2007**, *292*, 165–172.
(50) Drapeau, J.; Verdier, M.; Touraud, D.; Kröckel, U.; Geier, M.; Rose, A.; Kunz, W. *Chem. Biodivers.* **2009**, *6*, 934–947.
(51) Bonini, M.; Berti, D.; Di Meglio, J. M.; Almgren, M.; Teixeira, J.; Baglioni, P. *Soft Matter* **2005**, *1*, 444–454.
(52) Tucker, I.; Penfold, J.; Thomas, R.; Bradbury, R.; Grillo, I. *Langmuir* **2009**, *25*, 4934.
(53) Lee, C. T.; Smith, K. A.; Hatton, T. A. *Langmuir* **2009**, *25*, 13784–13794.
(54) Warr, G. G.; Sen, R.; Evans, D. F.; Trend, J. E. *J. Phys. Chem. B* **1988**, *92*, 774–783.
(55) Lindner, P.; Zemb, T. *Neutrons, X-ray and Light: Scattering Methods Applied to Soft Condensed Matter*; North Holland: Amsterdam, 2002.
(56) Fritz, G.; Bergmann, A.; Glatter, O. *J. Chem. Phys.* **2000**, *113*, 9733–9740.
(57) Abezgauz, L.; Kuperkar, K.; Hassan, P. A.; Ramon, O.; Bahadur, P.; Danino, D. *J. Colloid Interface Sci.* **2010**, *342*, 83–92.
(58) Collins, K. D. *Biophys. J.* **1997**, *72*, 65–76.
(59) Collins, K. D. *Biophys. J.* **1999**, *76*, A127–A127.
(60) Vlachy, N.; Jagoda-Cwiklik, B.; Vacha, R.; Touraud, D.; Jungwirth, P.; Kunz, W. *Adv. Colloid Interface Sci.* **2009**, *146*, 42–47.
(61) D'Errico, G.; Ortona, O.; Paduano, L.; Vitagliano, V. *J. Colloid Interface Sci.* **2001**, *239*, 264–271.
(62) Zielinski, R.; Ikeda, S.; Nomura, H.; Kato, S. *J. Chem. Soc. Faraday Trans. 1* **1988**, *84*, 151–163.
(63) Drifford, M.; Belloni, L.; Dubois, M. *J. Colloid Interface Sci.* **1987**, *118*, 50–67.
(64) Tartar, H. V. *J. Colloid Sci.* **1959**, *14*, 115–122.
(65) Zieliński, R. *J. Colloid Interface Sci.* **2001**, *235*, 201–209.
(66) Williams, E.; Sears, B.; Allerhand, A.; Cordes, E. H. *J. Am. Chem. Soc.* **1973**, *95*, 4871–4873.
(67) Uzu, Y.; Nakagawa, J.; Yokoi, M. *Bull. Chem. Soc. Jpn.* **1986**, *59*, 2891–2892.
(68) Yakovlev, D.; Boek, E. S. *Langmuir* **2007**, *23*, 6588–6597.
(69) Manet, S.; Karpichev, Y.; Bassani, D.; Kiagus-Ahjmad, R.; Oda, R. *Langmuir* **2010**, *26*, 10645–10656.
(70) Guinier, A.; Fournet, G. *Small Angle Scattering of X-ray*; Wiley: New York, 1955.
(71) Higgins, J. S.; Benoit, H. C. *Polymers and Neutron Scattering*; Clarendon: Oxford, England, 1994.
(72) Pedersen, J. S. *Adv. Colloid Interface Sci.* **1997**, *70*, 171–210.
(73) Guinier, A. *Ann. Phys.* **1939**, *12*, 161–237.
(74) Hayter, J. B.; Penfold *J. Mol. Phys.* **1981**, *42*, 109–118.
(75) Hansen, J. P.; Hayter, J. B. *Mol. Phys.* **1982**, *46*, 651–656.
(76) Bergstrom, M.; Pedersen, S. *Phys. Chem. Chem. Phys.* **1999**, *1*, 4437–4446.
(77) Chen, S. H.; Sheu, E. Y.; Kalus, J.; Hoffmann, H. *J. Appl. Crystallogr.* **1988**, *21*, 751–769.
(78) Hassan, P. A.; Fritz, G.; Kaler, E. W. *J. Colloid Interface Sci.* **2003**, *257*, 154–162.
(79) Ashcroft, N. W.; Lekner *J. Phys. Rev.* **1966**, *145*, 83–90.